OMICS A Journal of Integrative Biology
Volume 19, Number 5, 2015
© Mary Ann Liebert, Inc.
DOI: 10.1089/omi.2015.0009

Blood Metabolome Changes Before and After Bariatric Surgery: A ^{1}H NMR-Based Clinical Investigation

Thiago I.B. Lopes,[1] Bruno Geloneze,[2] José C. Pareja,[2] Antonio R. Calixto,[2] Márcia M.C. Ferreira,[1] and Anita J. Marsaioli[1]

Abstract

Excessive body fat and obesity have adverse health effects and result in significant morbidity such as type 2 diabetes mellitus. The health burden of obesity can be reduced with the Roux-en-Y gastric bypass (RYGB) weight-loss bariatric surgery. Little is known on the molecular changes that occur at the metabolome level before and after bariatric surgery, with a view to clinical biomarker development. Hence, we employed a metabolomics approach in 10 obese diabetic patients who underwent bariatric surgery. Metabolomics data were obtained by T_2- and diffusion-edited hydrogen nuclear magnetic resonance (^{1}H NMR) spectra to monitor the metabolic and lipoprotein profiles, and gas chromatography-mass spectrometry (CG-MS) to access the fatty acid profile before and 12 months after RYGB. Using hierarchical partial least squares discriminant analysis, we found that RYGB induces several key metabolic alterations associated with glucose homeostasis, as well as fatty acid and amino acid metabolism. The levels of lactate (Krebs' intermediate cycle) decreased after RYGB. The leucine, isoleucine, valine, lactate, and glucose levels were higher in the samples before RYGB ($p < 0.05$). Additionally, the levels of very low-density lipoprotein, unsaturated lipids, and N-acetyl-glycoprotein were higher before RYGB. By contrast, levels of the high-density lipoprotein and phosphatidylcholine were higher after bariatric surgery. These results collectively offer important holistic integrative biology data to develop future clinically relevant metabolomics biomarkers related to bariatric surgery in connection with obesity.

Introduction

OBESITY IS CHARACTERIZED BY EXCESSIVE BODY FAT with adverse health effects, resulting in co-morbidities, including type 2 diabetes mellitus (T2DM). Recently, Roux-en-Y gastric bypass (RYGB) weight-loss surgery has emerged as an effective and safe treatment for obesity and T2DM, with successful results in 50%–80% of cases (Buchwald et al., 2009). A retrospective study of approximately 10,000 individuals who underwent gastric bypass surgery revealed that mortality related to diabetes decreased by over 90% (Adams et al., 2007). The diabetes remissions occurred within days, which is relatively rapid and could not be fully explained by weight loss (Morinigo et al., 2006). Weight loss induced by RYGB leads to improvement in insulin resistance and pancreatic β-cell function by mechanisms that are weight loss-dependent and -independent (Geloneze et al., 2001). The effects of RYGB on T2DM remission have been associated with enhanced levels of the incretin hormones glucagon-like peptide 1 and glucose-dependent insulinotropic peptide; however, the exact mechanism is unclear (Catalan et al., 2007). RYGB also results in significant metabolic changes, such as better hormonal responses, decreasing levels of inflammatory markers, and lipid metabolism alteration (Catalan et al., 2007; Lima et al., 2010).

Long-term studies of RYGB are challenging because they depend on many interconnected variables, including caloric restriction, reduced adipose mass, diminished nutrient absorption, gut hormone and endogenous microbiota alteration, and metabolic adaptations (Friedrich et al. 2012; Laferrère et al., 2011; Lindqvist et al., 2013, Mutch et al., 2009). Several studies have demonstrated that the target metabolomics approach, using gas chromatography/mass spectrometry (GC-MS) and tandem mass spectrometry, successfully generate new data regarding the metabolic modifications associated with RYGB (Khoo et al., 2013; Laferrère et al., 2011; Lindqvist et al., 2013, Mutch et al., 2009). To the best of our knowledge, the application of NMR to RYGB metabolite profiling has not been mentioned.

[1]Chemistry Institute, and [2]Laboratory of Investigation on Metabolism and Diabetes, Universidade Estadual de Campinas (UNICAMP), Campinas, São Paulo, Brazil.

Metabolomics comprises the quantitative assessment of ''all metabolites'' (small molecules) within a biological system. This approach has been applied successfully to several research topics, such as environmental and biological systems and clinical and condition diagnosis (Lindon et al., 2003). Mass spectrometry and NMR are the two main analytical platforms employed in metabolomics research; however, both have different strengths and weaknesses (Ludwig et al., 2010; Patti et al., 2012). NMR-based metabolomics has a number of unique advantages because it is nondestructive and nonbiased, does not require separations or chemical derivatization, and allows the identification of novel compounds (Lindon et al., 2003; Wishart, 2008).

Hydrogen nuclear magnetic resonance (^{1}H NMR) spectra of blood plasma are marked by broad signals from macromolecules, such as proteins and lipoproteins (Ala-Korpela et al., 2007), which are frequently physically removed or suppressed by spin-echo sequences in metabolomics studies (Tiziani et al., 2008). Several studies have employed diffusion-edited ^{1}H NMR spectra to access lipoprotein profiles without sample pretreatment or separation of the lipoproteins (Ala-Korpela et al., 1994; Dyrby et al., 2005; Otvos et al., 1992; Petersen et al., 2005). ^{1}H NMR is a spectroscopic technique widely used in metabolomics, able to analyze biofluids and biological tissues with minimal sample preparation (Lindon et al., 2003). ^{1}H NMR is also able to detect polar and nonpolar metabolites with high or low molar mass. The technique provides a rapid, nondestructive, and highly reproducible analysis (Lindon et al., 2008). The main disadvantages of ^{1}H NMR is the cost of the equipment and its maintenance. The FA profile has been routinely monitored by GC-MS, the approach shows high detectability, repeatability, good linear correlation, and also identification of the analytes, a huge advantage when compared to more traditionally methods as GC-FID (Rodriguez et al., 2010).

Metabolomics investigations frequently employ multivariate analysis, but, in some cases, the large variable ensemble produces ''megavariate'' data. Traditional multivariate analysis provides plots and lists of loadings, weights, and coefficients that tend to blur and hamper the overall analysis. To solve such issues, the two main options are: selection of hierarchical variables to reduce the dataset or partition of the variables into blocks, and the application of hierarchical data analysis (Eriksson et al., 2002). Employment of hierarchical partial least square discriminant analysis (HiPLS-DA) can extract in-depth metabolic information from the RYGB procedure by an untargeted metabolomics approach, using three different data subsets: i) T_2- and ii) diffusion-edited ^{1}H NMR spectra to monitor the metabolic and lipoprotein profile, and iii) GC-MS to access the fatty acid (FA) profile.

Material and Methods

Chemicals

The deuterium oxide (D_2O 99.9%) was from the Cambridge Isotope Laboratory; the 2,2,3,3-d_4-3-(trimethylsilyl) propionic acid (TMSP) was from Acros Organics (Brazil, São Paulo); the monobasic potassium phosphate (KH_2PO_4) and dibasic potassium phosphate (K_2HPO_4) were obtained from Merck (Brazil, São Paulo). A Supelco 37-component FA methyl esters mix was acquired from Sigma-Aldrich (Brazil, São Paulo), and the nonadecanoic acid (C19:0), oleic (C18:1), linoleic (C18:2n6), and α-linolenic (C18:2n3) methyl esters were purchased from Acros.

Patients

Ten obese diabetic individuals (BMI = 32.38 ± 2.11 kg.m^{-2}) underwent RYGB surgery. The blood samples were collected after overnight fasting before and 12 months after surgery. The protocol was approved by the Institutional Review Board and the Brazilian Health Regulatory Agency. The data were collected according to the Good Clinical Practice Guidelines of the Declaration of Helsinki, and informed consent was obtained from all individuals.

Plasma collection and storage

Blood samples were collected from ten patients in Na_2EDTA (1.0 mg·mL^{-1}). The plasma samples were obtained by centrifugation at 800 *g* for 15 min, and the aliquots were transferred to polypropylene tubes and stored at –80°C until assayed.

Clinical parameters

The high-density lipoprotein (HDL) cholesterol and triglyceride (TG) levels were determined by enzymatic methods. The low-density lipoprotein (LDL) cholesterol level was calculated using the Friedewald method. The plasma glucose was measured by the glucose oxidase technique (Beckman Glucose Analyzers; Beckman, Fullerton, CA).

Sample preparation for NMR analysis

The plasma (400 μL) was mixed with phosphate buffer prepared in deuterium oxide (200 μL; pH = 7.4; 50 mmol·L^{-1} with 1.0 mmol·L^{-1} of TMSP). The mixture was homogenized in a vortex and centrifuged (10,000 *g* for 20 min at 4°C). Part of the supernatant (500 μL) was transferred to 5-mm NMR tubes. Duplicates of all plasma samples were prepared.

Acquisition and processing of the ^{1}H NMR spectra

The experiments were carried out without spinning at 25°C using an automated NMR ICON sample changer on a Bruker Avance DRX 400 (B_0 = 9.4 T) spectrometer equipped with a 5 mm TBI ^{1}H/^{13}C probe. T_2-edited and diffusion-edited ^{1}H NMR spectra were acquired for each sample. The T_2-edited ^{1}H NMR spectra were acquired using the Carr-Purcell-Meiboom-Gill pulse sequence (CPMG) to enhance the contribution of low-molecular-weight metabolites and PRESAT to suppress the water signal. The following parameters were used: 300 μs of evolution time and 600 ms of total spin-spin relaxation delay, with an accumulation of 64 scans. The magnetic field homogeneity was optimized for each sample. The diffusion-edited ^{1}H NMR spectra were acquired using Stimulated Echo experiment using bipolar gradients and WATERGATE (stebpgp) to obtain the lipoprotein spectral profiles. The WATERGATE 3-9-19 pulse sequence was used to suppress the water signal. A sine-shaped gradient pulse of 90% maximum strength, with 2.0 ms of duration (little delta), was followed by a delay (big delta) of 100 ms to allow the eddy currents to decay. This gradient strength was appropriate to attenuate the NMR peaks from

the fast-diffusing molecules (small molecules). The delay for the binomial water suppression was set at 17.0 μs, the gradient pulse was 1.0 ms, and the spectra were acquired with 32 scans.

The remaining acquisition parameters were as follows: spectral width, 6.0 kHz; data size, 32 k; acquisition time, 2.73 s; constant receiver gain, 203 and relaxation delay, 5.0 s. The data processing included zero filling to 128 k, line broadening multiplication by 1.0 (T_2-edited ^{1}H NMR) and 3.0 Hz (diffusion-edited ^{1}H NMR) and Fourier-transformation. All of the spectra were phase- and baseline-corrected and referenced to TMSP at 0.000 ppm and to the methyl resonance of lipoproteins at 0.800 ppm using TopSpin software (v3.1, Bruker Biospin). Heteronuclear single quantum coherence spectroscopy (2D ^{1}H-^{13}C HSQC), homonuclear total correlation spectroscopy (selective 1D ^{1}H-^{1}H TOCSY), and correlation spectroscopy (2D ^{1}H-^{1}H COSY) were performed to confirm the chemical shift assignments using Bruker's available sequences.

GC-MS acquisition and processing

The lipids were extracted from 100 μL of plasma applying a modified Folch's methodology (Folch et al., 1957; Iverson et al., 2001). The FA were converted to their respective FA methyl esters (FAME) as described by Croset et al. (2000), and the selected ion monitoring chromatograms were obtained as described by Lopes et al. (2013). The experiments were carried out using an Agilent-6890 series equipped with a Hewlett Packard-5973 mass selective detector. FAME standards were used to confirm the assignments.

Chemometrics analysis

The data sets were individually aligned by the MATLAB ICOSHIFT tool, using a target spectrum/chromatogram (randomly selected) as reference and selected intervals as the shifting guide (Savorani et al., 2010). The NMR data were reduced five times. The spectra and chromatograms were smoothed using a boxcar method with a window size of 5 pt for the NMR data and 7 pt for the GC-MS data. Principal component analysis (PCA) was performed (on the mean-centred data) to visualize the general structure of each block and detect any abnormalities. PCA models were applied on four independent blocks of data: Block X1, the aliphatic region of the T_2-edited ^{1}H NMR spectra; Block X2, the aromatic region of the T_2-edited ^{1}H NMR spectra; Block X3, the diffusion-edited ^{1}H NMR spectra and Block X4, the GC-MS chromatograms. The T_2-edited ^{1}H NMR spectral data were divided into two blocks to avoid overestimation of the aliphatic region significance. The training and test sets (containing approximately 2/3 and 1/3 of the total samples, respectively) were created using the distance-based optimal routine designed for MATLAB (Marengo and Todeschini, 1992), and the models were constructed with the training samples to the mean-centred data (the duplicates were always kept together in the training or in the test sets).

An optimal number of the principal components (PC) was selected for each model by scree plot analysis. The presence of outliers was evaluated by the Q residual versus the Hotelling's T^2 graph. All of the PCs contained in each PCA base-level model were combined to build the top-level ''super variables.'' The HiPLS-DA was performed on auto-scaled data, and cross-validation was used to select the appropriate number of latent variables (LV). The dataset was divided into Venetian blinds, and two validation runs (with 4 and 5 samples in the cross validation groups) were applied, providing similar results. The class threshold was selected when the number of false positives and false negatives were minimized, and these values corresponded to the intersection of the specificity and the sensitivity lines. The analyses were performed using the Classification toolbox for MATLAB (freeware, from Ballabio and Consonni, 2013).

Results

Clinical parameters

Ten volunteers were monitored before and 12 months after the RYGB, showing marked weight loss and metabolic profile improvement (Table 1). The body-mass index (BMI), fat mass, percentage of body fat, triglyceride (TG), and glucose levels decreased, whereas high-density lipoprotein (HDL) increased significantly. However, minor changes were observed in the waist–hip ratio and cholesterol low-density lipoprotein (LDL) levels.

Base-level PCA Model

Four blocks (X_1–X_4) were constructed on the base-level: X_1 Block, aliphatic region of T_2-edited ^{1}H NMR spectrum; X_2 Block, aromatic region of T_2-edited ^{1}H NMR spectrum; X_3 Block, diffusion-edited ^{1}H NMR spectrum, and X_4 Block, GC-MS chromatograms. The blocks were individually interpreted by their loading values selected in the HiPLS-DA (next section). The main parameters of the base-level models are given in Table 2. The score plots of the first two principal components of all four blocks, the ROC curves demonstrating that the models are sensitive (ability to correctly recognize samples belonging to that class) and specific (ability to reject the samples of all other classes), and other relevant graphs are shown in the supplementary material.

Table 1. Clinical Parameters

	Before RYGB[a]	*After RYGB*[a]	p
Weight (kg)	85.51 ± 10.46	67.22 ± 7.78	**< 0.001**
BMI (kg/m^2)	32.38 ± 2.11	25.48 ± 1.85	**< 0.001**
Waist–hip ratio	0.98 ± 0.08	0.91 ± 0.07	0.062
Fat mass (kg)	27.80 ± 5.60	14.86 ± 4.69	**< 0.001**
% Body fat	31.47 ± 7.48	22.13 ± 6.50	**0.008**
Cholesterol (mg/dL)	193.80 ± 24.56	171.70 ± 29.72	0.087
HDL (mg/dL)	36.90 ± 10.51	49.30 ± 13.40	**0.033**
LDL (mg/dL)	104.10 ± 27.32	98.20 ± 26.57	0.630
TG (mg/dL)	250.50 ± 100.33	120.90 ± 51.50	**0.002**
Glucose (mg/dL)	159.80 ± 61.43	100.00 ± 22.94	**0.010**
HOMA-IR	10.961 ± 8.314	1.089 ± 0.526	**0.002**

[a]Values are the means ± SD; the means were compared using Student's paired *t*-test with equal variances assumed, $p < 0.05$ was considered significant.

BMI, body-mass index; HDL, high-density lipoprotein; HOMA, homeostasis mode assessment insulin resistance; LDL, low-density lipoprotein; TG, triglycerides.

Boldface = statistically significant values.

TABLE 2. MAIN PARAMETERS OF PCA MODELS

Parameters	*Block X1: aliphatic region of T_2-edited ^1H NMR*	*Block X2: aromatic region of T_2-edited ^1H NMR*	*Block X3: Diffusion-edited ^1H NMR*	*Block X4: GC-MS*
Training samples	28	28	28	28
Test samples	12	12	12	12
Variables	0.65–4.77 ppm[a] (6636 points)	6.78–8.10 ppm (2305 points)	0.50–3.50 ppm (2624 points)	26.19 min[b] (3543 points)
Number of PCs	6	4	4	3
X-variance	96.3%	68.9%	96.8%	98.6%
Error on CV	7.0%	19.0%	15.0%	7.0%

[a]The regions between 3.20–3.40 and 3.60–3.70 corresponding to the free-H_2EDTA^{2-} (added in the sample collection) were removed from the analysis; [b]The region between 24.75–25.50 min corresponding to C19:0 (the internal standard) was also removed from the analysis.

Top-level PLS-DA model

All significant base-level PC from the PCA model were combined to build the ''super variables'' (Fig. 1); for example, t_1X_1 represents the first score value (t_1) from the first block (X_1). The HiPLS-DA model was constructed with four LV and explained 25.0% and 44.5% of the variance on the X and Y-data, respectively. The error rate was equal to 0.0%, 4.0%, and 0.0% in the fitting data, cross-validation, and external sample predictions, respectively. The ROC curve and other relevant parameters and graphs of the PLS-DA model are shown in the supplementary figures (supplementary material is available online at www.liebertpub.com/omi). The scores plot (Fig. 2a) shows that samples before RYGB had rather positive scores on the LV1. The loading plot shows the contribution of the ''super variables'' in the observed clustering of the scores plot (Fig. 2b). The most significant ''super variables'' on HiPLS-DA model (t_2X_1, t_2X_2, t_2X_3 and t_2X_4)

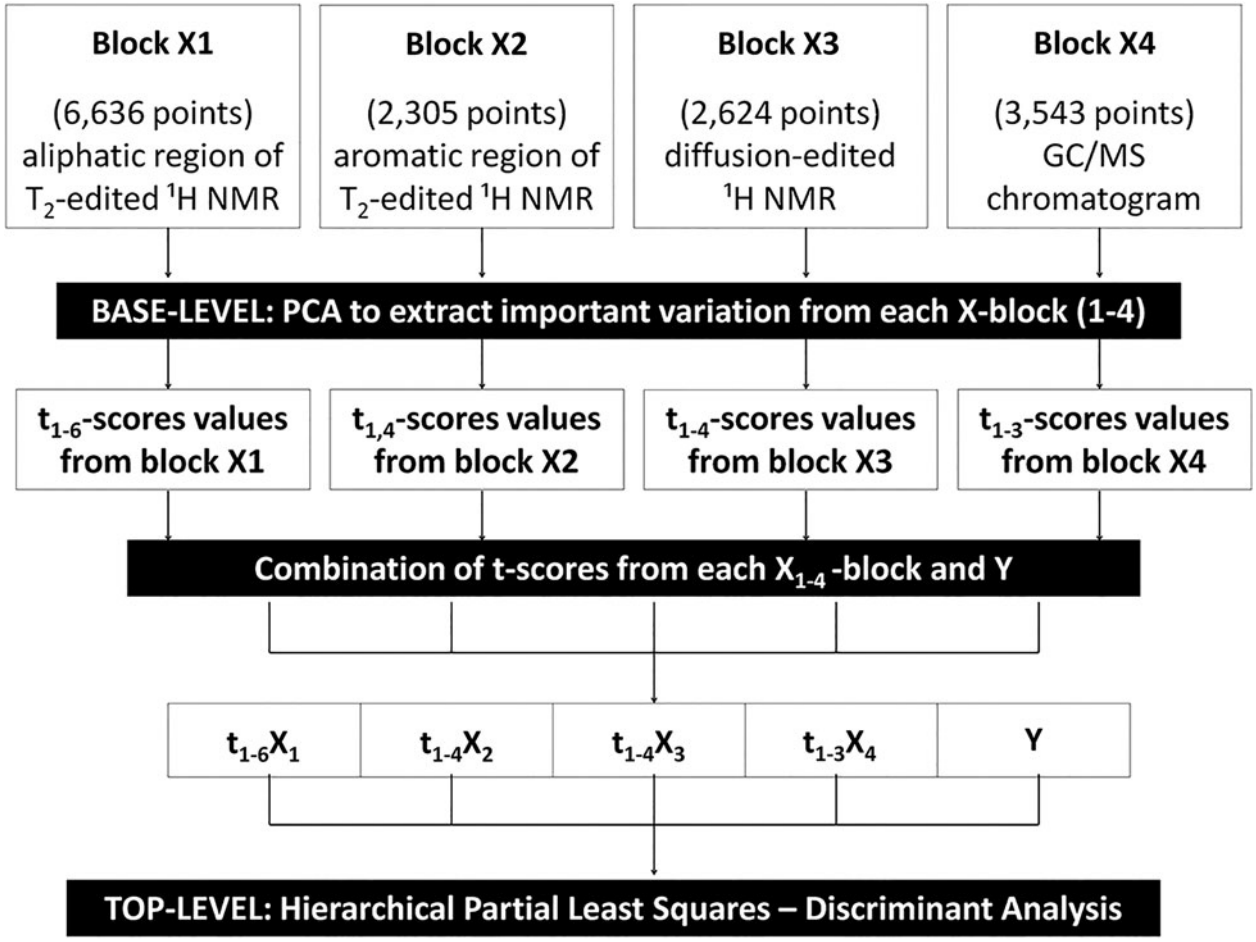

FIG. 1. Schematic overview of a hierarchical modeling procedure. Each of the four blocks ($X_{1–4}$) was summarized by means of 6, 4, 4, and 3 principal components from the base-level PCA models. The Y-matrix of the top-level corresponds to a dummy matrix of the classes (containing 0 and 1).

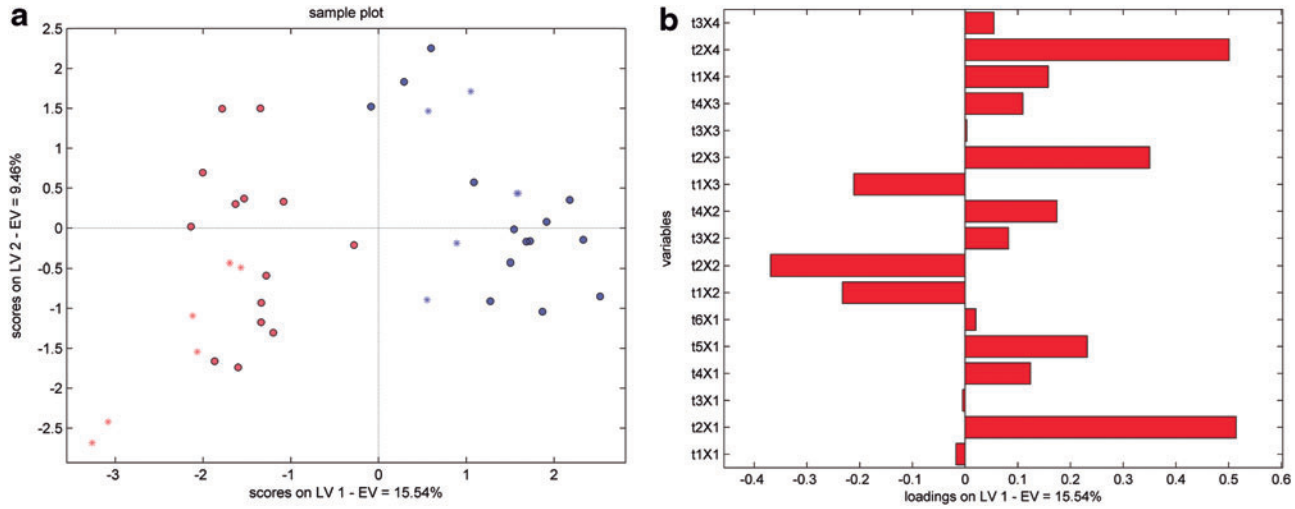

FIG. 2. **(a)** Scores plot and **(b)** loadings plot from the HiPLS-DA model (LV = 2; 35.0% and 44.5% of the explained variance in the X- and Y-data, respectively). The before RYGB samples are colored in *blue* and the after RYGB samples in *red*, training (•) and test (∗) samples; the ''super variable'' construction (t_nX_n) is explained in Figure 1.

were selected based on the distribution of Wilks' lambda and retaining variables with values below 0.800. The loadings of the base-level PCA models are shown in Figs. 3–6b. One of the highlighted ''super variables'' (t_2X_2) had negative values, and the corresponding loadings were multiplied by −1. Thus, the positive loadings were associated with compounds that decreased after RYGB.

Spectra and chromatograms

Representative ^{1}H NMR spectra and GC-MS chromatograms are shown in Figures 3–6a. The highlighted resonances in the chemometrics analysis were assigned according to NMR data in the literature and were confirmed by 1D selective ^{1}H-^{1}H TOCSY, ^{1}H-^{13}C HSQC-edited. The highlighted peaks were assigned by full mass spectra and standard co-injections.

Metabolic profile by the T_2-edited ^{1}H NMR

The T_2-edited ^{1}H NMR spectra were divided into two regions: the aliphatic (Block X_1, Fig. 3) and the aromatic regions (Block X_2, Fig. 4). The leucine, isoleucine, valine, threonine, lactate, and glucose levels were higher in the samples before RYGB. The levels of acetate, glutamine/glutamate, methylamine, dimethylamine, O-acetyl-carnitine,

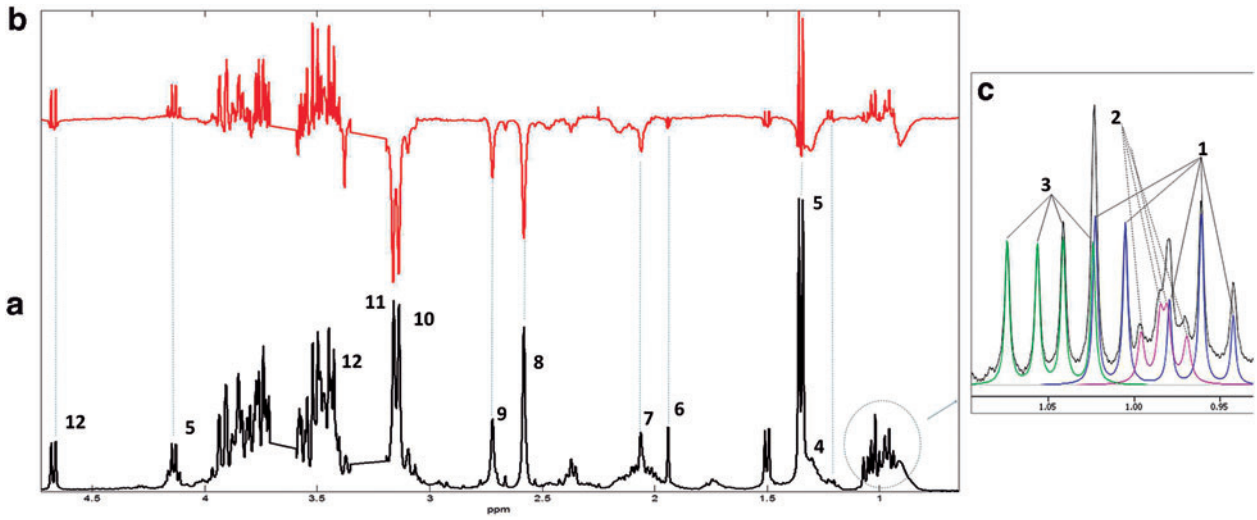

FIG. 3. **(a)** Representative plasma partial ^{1}H NMR T_2-edited spectrum showing the aliphatic region before RYGB, **(b)** the PC2 loadings of the base-level PCA model from the X_1 block (t_2X_1 ''super variable''), and **(c)** the deconvolution of the methyl resonances from the BCAA. The resonances associated with the positive loadings correspond to the compounds found in higher amounts in the samples before RYGB. The breaks at (3.20–3.40 and 3.60–3.70 ppm) correspond to free-H_2EDTA^{2-} resonance removal from the chemometrics analysis. 1, isoleucine (*blue line*); 2, leucine (*pink line*); 3, valine (*green line*); 4, threonine; 5, lactate; 6, acetate; 7, glutamine/glutamate; 8, methylamine; 9, diethylamine; 10, O-acetyl-carnitine; 11, carnitine; 12, glucose.

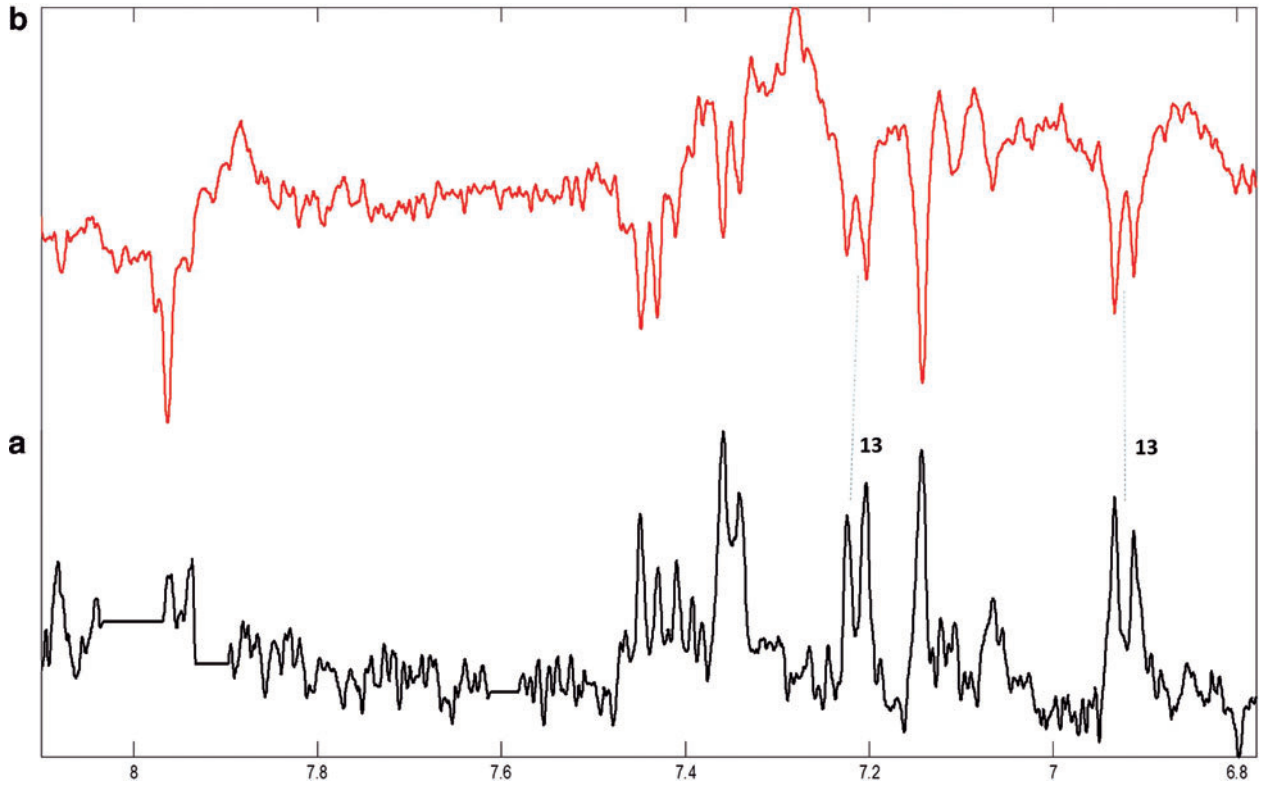

FIG. 4. **(a)** Representative plasma partial ^{1}H NMR T_2-edited spectrum showing the aromatic region before RYGB, and **(b)** the PC2 loadings of the base-level PCA model from the X_2 block (t_2X_2 ''super variable''). The resonances associated with the positive loadings corresponded to compounds found in higher levels in the samples before RYGB. 13, *p*-cresol.

and carnitine were higher after RYGB. The aromatic region showed that the p-cresol levels were higher after RYGB.

Lipoprotein profiles by the diffusion-edited ^{1}H NMR

The PLS-DA loadings show several differences in the lipid profile (Block X_3, Fig. 5). The levels of VLDL, LDL, unsaturated lipids, and N-acetyl-glycoprotein were higher before RYGB. Higher levels of HDL and phosphatidylcholine (PtdCho) were associated with samples after RYGB. The results of the NMR spectral analyses are in good agreement with those of the enzymatic methods (Table 1).

Fatty acid profile by GC-MS

The PLS-DA loadings showed several differences before and after RYGB in the FA profile (Block X_4, Fig. 6), such as decreasing levels of polyunsaturated FA (C18:3n3, C18:2n6,

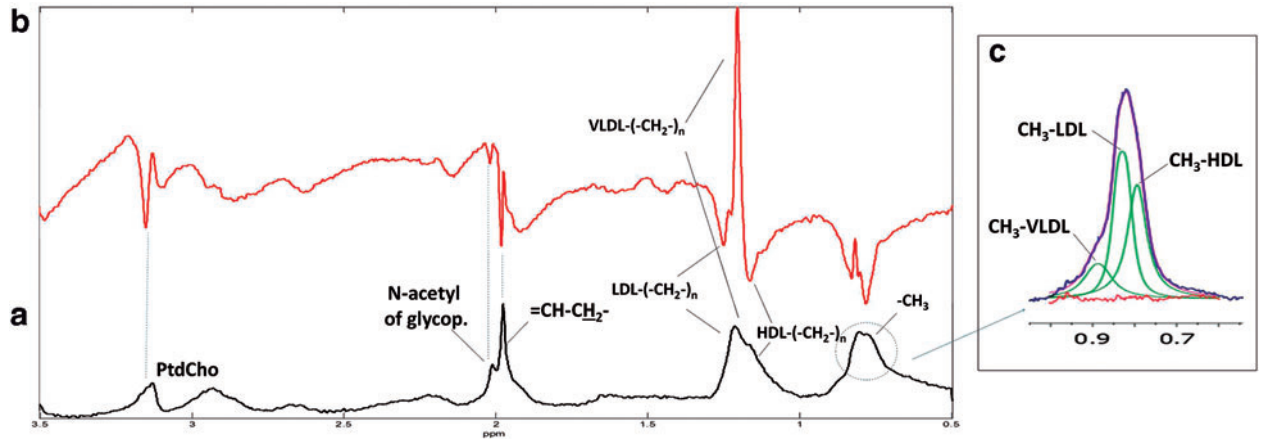

FIG. 5. **(a)** Representative plasma partial ^{1}H NMR diffusion-edited spectrum before RYGB, **(b)** the PC2 loadings of the base-level PCA model of the X_3 block (t_2X_3 ''super variable''), and **(c)** expansion and deconvolution of the methyl resonances from lipids. The resonances associated with the positive loadings corresponded to compounds found in higher levels in the samples before RYGB. HDL, high-density lipoprotein; LDL, low-density lipoprotein; N-acetyl of glicop, N-acetyl of glycoproteins; PtdCho, phosphatidylcholine; VLDL, very low-density lipoprotein.

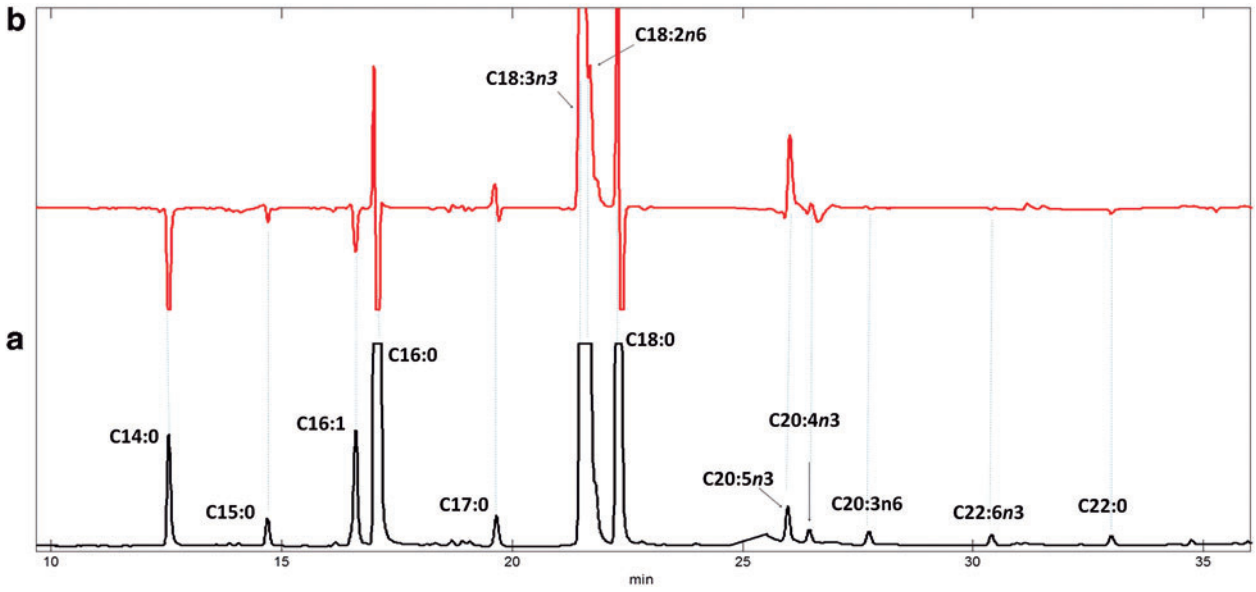

FIG. 6. **(a)** Representative plasma gas chromatogram-mass before RYGB and **(b)** the PC2 loadings of the base-level PCA model from the X_4 block (t_2X_4 ''super variable''). The resonances associated with the positive coefficients correspond to compounds detected at higher levels before RYGB. C14:0, myristic acid; C15:0, pentadecanoic acid; C16:1, palmitoleic acid; C16:0, palmitic acid; C17:0, margaric acid; C18:3*n*3, α-linolenic acid; C18:2*n*6, linoleic acid; C18:0, stearic acid; C20:5*n*3, eicosapentaenoic acid; C20:4*n*6, arachidonic acid; C20:3*n*6, dihomo-γ-linolenic acid; C22:6n3, cervonic acid; C22:0, behenic acid.

C20:5n3, C20:4n3, C20:3n6, and C22:6n3) and increasing levels of saturated FA (C14:0, C15:0, C16:0, C17:0, C18:0, and C22:0).

Discussion

OMICS research has become a mainstay form of investigation worldwide, including in Africa and resource-limited countries (Dandara et al., 2014). The results suggest that RYGB induces several alterations associated with glucose homeostasis and fatty acid metabolism. HiPLS-DA was successful in integrating different chemical information from the NMR and GC-MS data, providing an extremely large and unbiased overview of this surgical procedure.

Metabolites related to energy homeostasis

The observed decreasing levels of lactate (Krebs' intermediate cycle) after RYGB could be assigned to the decreasing glucose input and to consequent increasing gluconeogenesis. Increasing plasma acetate concentration revealed an enhanced FA oxidation due to caloric restrictions imposed by RYGB. These observations corroborate previously reported results by Mutch et al. (2009), indicating that RYGB has profound effects in energy homeostasis, by shifting the gluconeogenesis and the tricarboxylic acid cycle.

One of the most accepted theories to explain the relationship between lipid metabolism and insulin resistance is the lipotoxicity mechanism, in which an accumulation of lipids occurs in insulin-sensitive tissues, such as skeletal muscle. Muoio et al. (2007) suggested that an alternative mechanism, in which the rate of oxidation of fatty acids exceeds the capacity of the tricarboxylic acid cycle and leads to accumulation of such intermediates as carnitine, may be associated with insulin resistance. L-carnitine is involved in the transportation of activated fatty acids from the cytosol into the mitochondria, where oxidation occurs (L-acetyl-carnitine intermediates of the acetyl-CoA transportation into mitochondria during the oxidation of fatty acids). Additionally, it has never been suggested that RYGB induces higher methylamine and dimethylamine levels. However, further investigations are necessary.

Amino acids

Amino acid and carbohydrate metabolic interactions are well known. Moreover, amino acids directly contribute to ''de novo'' synthesis of glucose via gluconeogenesis and participate in the glucose recycling via the glucose–alanine cycle (Layman and Baum, 2004). Previous reports have demonstrated that branched-chain amino acid (BCAA) levels are higher in obese and diabetic individuals compared with lean and nondiabetic individuals, respectively (Newgard et al., 2009). The observed decreasing plasma levels of valine, leucine, and isoleucine after RYGB are in agreement with previously reported data, indicating that the plasma BCAA levels decrease approximately 35% following gastric bypass surgery (Jung et al., 2012; Laferrère et al., 2011). These observations could be explained by higher alanine and glutamine levels in the skeletal muscles, which maintain glucose homeostasis through the glucose–alanine cycle. BCAA and hyperlipidemia are related to insulin resistance, that decreased significantly, as demonstrated by the HOMA (homeostatic model assessment). This result was most likely due to the interplay between the BCAA and lipid reductions after surgery (Batch et al., 2013; Morris et al., 2012). Lower BCAA levels might reflect nutrient intake decrease, although

the plasma samples were collected after overnight fasting to minimize the dietary influence. Additionally, it has never been suggested that RYGB induces lower threonine levels. However, further investigations are necessary.

Metabolites related to gut microbiota

Alterations in the gut microbiota were reported by Mutch et al., with the finding of an increasing amount of plasma p-cresol and indole after a 3–6 month period after RYGB in morbidly obese females (Mutch et al., 2009). We have demonstrated that the *p*-cresol levels remain high 12 months after RYGB. Recent metabolic studies have demonstrated that gut microflora are closely associated with diet-induced obesity and that consumption of a high-fat diet results in decreasing gut bacterial levels (Jung et al., 2012). It is relatively difficult to demonstrate whether the microbiota alteration arises from RYGB or by changes in the intestinal permeability.

Lipoprotein profile

The plasma ^{1}H NMR spectra have signal overlapping of low- and high-molecular-weight compounds, and the fast diffusion signals (small molecules) are cancelled by the diffusion-edited ^{1}H NMR, which simplifies the spectra. Lipoprotein methyl groups have slightly different chemical shifts due to magnetic susceptibility effects caused by their different hydrodynamic radii (Liu et al., 2002). Lipoprotein absolute concentrations were not obtained here by the diffusion-edited ^{1}H NMR spectra. However, we have extracted information regarding the lipoprotein lipid profiles with no sample workup, and the results were confirmed by traditional analyses using enzymatic methods. Therefore, the NMR approach is faster and decreases sample amount requirements and analytical costs.

This approach showed that the VLDL, unsaturated lipids, and N-acetyl-glycoprotein levels decreased with RYGB. The decreasing levels of unsaturated lipids are in consensus with a previous report (Williams et al., 2007) and were confirmed by the GC-MS fatty acid profile. The decreasing levels of unsaturated lipids could indicate excessive lipid peroxidation and/or oxidative stress with RYGB (Williams et al., 2007). We also observed higher phosphatidylcholine and phosphocholine levels following RYGB, which is consistent with an increased HDL level, given that PtdCho is the predominant lipid (Duarte et al., 2007). Lower levels of N-acetyl-glycoproteins and higher levels of choline-containing phospholipids indicate lipid mobilization from non-adipose tissues. N-Acetyl-glycoprotein is an inflammatory marker (Bell et al., 1987), and its decreasing levels indicate a reduction of inflammatory processes.

Fatty acid profile

The slowing of the glucose metabolism switches energy consumption towards lipid oxidation and FA consumption (Barron et al., 1998). We observed that lower levels of essential FA (C18:3*n*3 and C18:2*n*6, nonsynthesized by humans and other animals) are higher before RYGB. After RYGB, the levels of polyunsaturated FA as C20:5*n3*, C20:4*n*6, C20:3*n*6, and C22:6n3 decreased, corroborating the hypothesis of excessive lipid peroxidation and/or oxidative stress after RYGB. Endogenous FAs (synthesized from carbohydrates as C14:0, C16:0, C18:0, and C22:0 (King et al., 2006)) are significantly higher after 12 months of RYGB. The most significant observations were the change in the odd carbon number FA (as C15:0 and C17:0) levels. These FA are synthesised by the endogenous microbiota, corroborating the hypothesis of a change in gut microbiota induced by RYGB (Liou et al., 2013).

Conclusion

This study provides a holistic approach in RYGB response. The combination of analytical methodologies and chemometrics analysis was successful in providing multiparametric metabolic responses, leading to a broader view of the metabolic network. The results revealed RYGB-associated changes in lipid metabolism, gut microbiota, and metabolites related to energy homeostasis, thereby highlighting the multifaceted nature of this metabolic surgery.

Acknowledgment

We thank the Fundação de Amparo à Pesquisa do Estado de São Paulo (Sao Paulo State Research Foudation—FAPESP, São Paulo, Brazil).

Author Disclosure Statement

The authors declare there are no conflicting financial interests.

References

Adams TD, Gress RE, Smith SC, et al. (2007). Longer mortality after gastric bypass surgery. N Engl J Med 357, 753–761.

Ala-Korpela M, Korhonen A, Keisala J, et al. (1994). ^{1}H NMR-based absolute quantitation of human lipoproteins and their lipid contents directly from plasma. J Lipid Res 35, 2292–2304.

Ala-Korpela M, Lankinen N, Salminen A, et al. (2007). The inherent accuracy of ^{1}H NMR spectroscopy to quantify plasma lipoproteins is subclass dependent. Atherosclerosis 190, 352–358.

Ballabio D, and Consonni V. (2013). Classification tools in chemistry. Part 1: Linear models. PLS-DA. Anal Methods 5, 3790–3798.

Barron JT, Barany M, Gu L, and Parrillo JE. (1998). Metabolic fate of glucose in vascular smooth muscle during contraction induced by noradrenaline. J Mol Cell Cardiol 30, 709–719.

Batch BC, Shah SH, Newgard CB, et al. (2013). Branched chain amino acids are novel biomarkers for discrimination of metabolic wellness. Metabolism 62, 961–969.

Bell JD, Brown JC, Nicholson JK, and Sadler PJ. (1987). Assignment of resonances for 'acute phase' glycoproteins in high resolution proton NMR spectra of human blood plasma. FEBS Lett 215, 311–315.

Buchwald H, Estok R, Fahrbach K, et al. (2009). Weight and type 2 diabetes after bariatric surgery: Systematic review and meta-analysis. Am J Med 122, 248–256.

Catalan V, Gomez-Ambrosi J, Ramirez B, et al. (2007). Proinflammatory cytokines in obesity: Impact of type 2 diabetes mellitus and gastric bypass. Obesity Surg 17, 1464–1474.

Croset M, Brossard N, Polette A, and Lagarde M. (2000). Characterization of plasma unsaturated lysophosphatidylcholines in human and rat. Biochem J 345, 61–67.

Dandara C, Huzair F, Borda-Rodriguez A, Chirikure S, Okpechi I, Warnich L, and Masimirembwa C. (2014). H3Africa and

the African life sciences ecosystem: Building sustainable innovation. OMICS 18, 733–739.

Duarte IF, Goodfellow BJ, Barros A, et al. (2007). Metabolic characterisation of plasma in juveniles with glycogen storage disease type 1a (GSD1a) by high-resolution ^{1}H NMR spectroscopy. NMR Biomed 20, 401–412.

Dyrby M, Petersen M, Whittaker AK, Lambert L, Nørgaard L, Bro R, and Engelsen SB. (2005). Analysis of lipoproteins using 2D diffusion-edited NMR spectroscopy and multi-way chemometrics. Anal Chim Acta 531, 209–216.

Eriksson L, Johansson E, Lindgren F, Sjöström M, and Wold S. (2002). Megavariate analysis of hierarchical QSAR data. J Computer-Aided Mol Design 16, 711–726.

Friedrich N, Budde K, Wolf T, et al. (2012). Short-term changes of the urine metabolome after bariatric surgery. OMICS 16, 612–620.

Folch J, Lees M, and Stanley GHS. (1957). A simple method for the isolation and purification of total lipids from animal tissues. J Biol Chem 226, 497–509.

Geloneze B, Tambascia MA, Pareja JC, Repetto EM, and Magna LA. (2001). The insulin tolerance test in morbidly obese patients undergoing bariatric surgery. Obesity Res 9, 763–769.

Iverson SJ, Lang SLC, and Cooper MH. (2001). Comparison of the Bligh and Dyer and Folch methods for total lipid determination in a broad range of marine tissue. Lipids 36, 1283–1287.

Jung JY, Kim IY, Kim YN, et al. (2012). ^{1}H NMR-based metabolite profiling of diet-induced obesity in a mouse mode. BMB Rep 45, 419–424.

Khoo CM, Muehlbauer MJ, Stevens RD, Pamuklar Z, Chen J, Newgard CB, and Torquati A. (2013). Postprandial metabolite profiles reveal differential nutrient handling after bariatric surgery compared with matched caloric restriction. Ann Surg 19, 1–5.

King IB, Lemaitre RN, and Kestin M. (2006). Effect of a low-fat diet on fatty acid composition in red cells, plasma phospholipids, and cholesterol esters: investigation of a biomarker of total fat intake. Am J Clin Nutr 83, 227–236.

Laferrère B, Reilly D, Arias S, et al. (2011). Differential metabolic impact of gastric bypass surgery versus dietary intervention in obese diabetic individuals despite identical weight loss. Sci Translat Med 3, 80–82.

Layman DK, and Baum JI. (2004). Dietary protein impact on glycemic control during weight loss. J Nutr 134, 968S–973S.

Lima MMO, Pareja JC, Alegre SM, et al. (2010). Acute effect of Roux-En-Y gastric bypass on whole-body insulin sensitivity: A study with the euglycemic-hyperinsulinemic clamp. J Clin Endocrinol Metab 95, 3871–3875.

Lindon JC, Holmes E, and Nicholson JK. (2003). So what's the deal with metabonomics? Anal Chem 75, 384–391.

Lindon JC, and Nicholson JK. (2008). Spectroscopic and statistical techniques for information recovery in metabonomics and metabolomics. Ann Rev Anal Chem 1, 45–69.

Lindqvist A, Spégel P, Ekelund M, Mulder H, Hedenbro LGJ, and Wierup N. (2013). Effects of ingestion routes on hormonal and metabolic profiles in gastric-bypassed humans. J Clin Endocrinol Metab 98, 856–861.

Liou AP, Paziuk M, Luevano Jr JM, Machineni S, Turnbaugh PJ, and Kaplan LM. (2013). Conserved shifts in the gut microbiota due to gastric bypass reduce host weight and adiposity. Sci Translat Med 5, 1–11.

Liu M, Tang H, Nicholson JK, and Lindon JC. (2002). Use of ^{1}H NMR-determined diffusion coefficients to characterize lipoprotein fractions in human blood plasma. Magnet Reson Chem 40, S83–S88.

Lopes TIB, Rimland CA, Nagassaki S, Geloneze B, and Marsaioli AJ. (2013). A chemometric model applied to fatty acid determination in blood. J Brazil Chem Soc 24, 1599–1605.

Ludwig C, and Viant MR. (2010). Two-dimensional J-resolved NMR spectroscopy: Review of a key methodology in the metabolomics toolbox. Phytochem Anal 21, 22–32.

Marengo E, and Todeschini R. (1992). A new algorithm for optimal, distance-based experimental design. Chemomet Intelligent Lab Systems 16, 37–44.

Morinigo R, Lacy AM, Casamitjana R, Delgado S, Gomis R, and Vidal J. (2006). GLP-1 and changes in glucose tolerance following gastric bypass surgery in morbidly obese Individuals. Obesity Surg 16, 1594–1601.

Morris C, O'Grada C, Ryan M, Roche HM, Gibney MJ, Gibney ER, and Brennan L. (2012). The relationship between BMI and metabolomics profiles: A focus on amino acids. Proc Nutr Soc 71, 634–638.

Muoio DM, and Koves TR. (2007). Lipid-induced metabolic dysfunction in skeletal muscle. Novartis Found Symp 286, 24–38.

Mutch DM, Fuhrmann JC, Rein D, Wiemer JC, Bouillot JL, Poitou C, and Clement K. (2009). Metabolite profiling identifies candidate markers reflecting the clinical adaptations associated with roux-en-y gastric bypass surgery. PLoS ONE 4, e7905–e7917.

Newgard CB, An J, Bain JR, Muehlbauer MJ, Stevens RD, Lien LF, et al. (2009). A branched-chain amino acid-related metabolic signature that differentiates obese and lean humans and contributes to insulin resistance. Cell Metab 9, 311–326.

Otvos JD, Jeyarajah EJ, Bennett DW, and Krauss RM. (1992). Development of a proton nuclear magnetic resonance spectroscopic method for determining plasma lipoprotein concentrations and subspecies distributions from a single, rapid measurement. Clin Chem 38: 1632–1638.

Patti GJ, Yanes O, and Siuzdak G. (2012). Innovation: Metabolomics: The apogee of the omics trilogy. Nature Rev Mol Cell Biol 13, 263–269.

Petersen M, Dyrby M, Toubro S, Engelsen SB, Norgaard L, Pedersen HT, and Dyerberg J. (2005). Quantification of lipoprotein subclasses by proton nuclear magnetic resonance-based partial least-squares regression models. Clin Chem 51, 1457–1461.

Rodriguez AR, Reglero G, and Ibañez E. (2010). Recent trends in the advanced analyses of bioactive fatty acids. J Pharm Biomed Anal 51, 305–326.

Savorani F, Tomasi G, and Engelsen SB. (2010). Icoshift: A versatile tool for the rapid alignment of 1D NMR spectra. J Magnet Reson 202, 190–202.

Tiziani S, Emwas AH, Lodi A, Ludwig C, Bunce CM, Viant MR, and Gunther UL. (2008). Optimized metabolite extraction from blood serum for ^{1}H nuclear magnetic resonance spectroscopy. Anal Biochem 377, 16–23.

Williams DB, Hagedorn JC, Lawson EH, et al. (2007). Gastric bypass reduces biochemical cardiac risk factors. Surg Obesity Related Dis 3, 8–13.

Wishart DS. (2008). Quantitative metabolomics using NMR. Trends Anal Chem 27, 228–237.

Address correspondence to:
Professor Anita J. Marsaioli
Chemistry Institute, Campinas
Universidade Estadual de Campinas (UNICAMP)
13083-970, São Paulo
Brazil

E-mail: anita@iqm.unicamp.br

Abbreviations Used

BCAA = branched-chain amino acid
BMI = body mass index
stebpgp = Stimulated Echo experiment using bipolar gradients and WATERGATE
GC-MS = gas chromatography-mass spectrometry
COSY = correlation spectroscopy
CPMG = Carr-Purcell-Meiboom-Gill pulse sequence
FA = fatty acid
FAME = fatty acid methyl esters
^{1}H NMR = hydrogen nuclear magnetic resonance
HDL = high-density lipoprotein
HiPLS-DA = hierarchical partial least squares discriminant analysis
HSQC = heteronuclear single quantum coherence spectroscopy
LDL = low-density lipoprotein
LV = latent variables
PC = principal components
PCA = principal component analysis
PtdCho = phosphatidylcholine
RYGB = Roux-en-Y gastric bypass
T2DM = type 2 diabetes mellitus
TG = triglyceride
TMSP = *2,2,3,3-d_4-3-*(trimethylsilyl) propionic acid
TOCSY = homonuclear total correlation spectroscopy
VLDL = very low-density lipoprotein